

Supporting Information of

CHARMM Force-fields with Modified Polyphosphate Parameters allow Stable Simulation of the ATP-Bound Structure of Ca²⁺-ATPase

Yasuaki Komuro^{§††}, Suyong Re[‡], Chigusa Kobayashi[†], Eiro Muneyuki[§] and Yuji Sugita^{††\$#*}

[§]Graduate School of Science and Engineering, Chuo University, 1-13-27, Kasuga, Bunkyo-ku, Tokyo 112-8551, Japan; [‡]RIKEN Theoretical Molecular Science Laboratory, 2-1, Hirosawa, Wako-shi, Saitama 351-0198, Japan; [†]RIKEN Advanced Institute for Computational Science, International Medical Device Alliance (IMDA) 6F, 1-6-5 Minatojima-minamimachi, Chuo-ku, Kobe, Hyogo 650-0047, Japan; ^{\$}RIKEN Quantitative Biology Center, International Medical Device Alliance (IMDA) 6F, 1-6-5 Minatojima-minamimachi, Chuo-ku, Kobe, Hyogo 650-0047, Japan; [#]RIKEN iTHES, 2-1, Hirosawa, Wako-shi, Saitama 351-0198, Japan.

List of contents

Table S1: Summary of the simulation systems.

- (a) MD simulations of E1•ATP
- (b) MD simulations of four ATP-bound proteins
- (c) REMD simulations of ATP in solution

Table S2: Atom names, types and partial charges of methyl triphosphate (MTP).

Figure S1. Potential energy profiles along the selected dihedral angles of MTP.

Figure S2. Time course of the selected structural parameters in 20 ns-MD simulations using mod-C27(ATP) with ion parameters developed by Merz, Jr.

Figure S3. A snapshot of ATP-binding site after 20ns-MD simulation using mod-C27(ATP) with ion parameters developed by Merz, Jr.

Figure S4. Root mean square deviations (RMSDs) of polyphosphate moiety of ATP for 5 ns MD simulations of ATP-bound proteins

Figure S5. Performance of REMD simulations using C27(ATP) and mod-C27(ATP).

Figure S6. Convergence of REMD simulations using C27(ATP) and mod-C27(ATP).

Figure S7. Comparison of calculated PMF with X-ray crystal structures.

Table S1. Summary of the simulation systems.

(a) MD simulations of E1•ATP

Number of atoms	378177
Number of water molecules	96099
Number of lipid molecules	535
Number of counter ions	295K ⁺ / 272Cl ⁻
ATP binding site	1ATP + 1Mg ²⁺
Ca ²⁺ binding site	2Ca ²⁺
P-domain	1K ⁺
Box size (Å ³)	140 × 140 × 200

(b) MD simulations of four ATP-bound proteins. In each protein, hydrogen atoms were added to the crystal structure using the VMD 1.9.1 tool set.¹ Cavities inside the protein were filled with water molecules using DOWSER.² The systems were solvated and neutralized with 150 mM KCl.

	Histidine permease (PDB: 1b0u)	RNA editing ligase MP52 (PDB entry: 1xdn)
Number of atoms	42410	41793
Number of protein atoms	4106	4232
Number of nucleotides	1ATP	1ATP
Number of water molecules	12727	12480
Number of ions	41K ⁺ , 39Cl ⁻	42K ⁺ , 35Cl ⁻ , 1Mg ²⁺
Box size (Å ³)	70 × 83 × 79	79 × 70 × 81
	Phosphoribosylamidoimidazole- succinocarboxamide synthase (PDB entry: 1obd)	α-skeletal muscle Actin (PDB entry: 2fxu)
Number of atoms	53229	63642
Number of protein atoms	4795	5617
Number of nucleotides	1ATP, 1AMP	1ATP
Number of water molecules	16086	19287
Number of counter ions	51K ⁺ , 45Cl ⁻ , 2Mg ²⁺	63K ⁺ , 54Cl ⁻ , 4Ca ²⁺
Box size (Å ³)	91 × 77 × 81	73 × 94 × 99

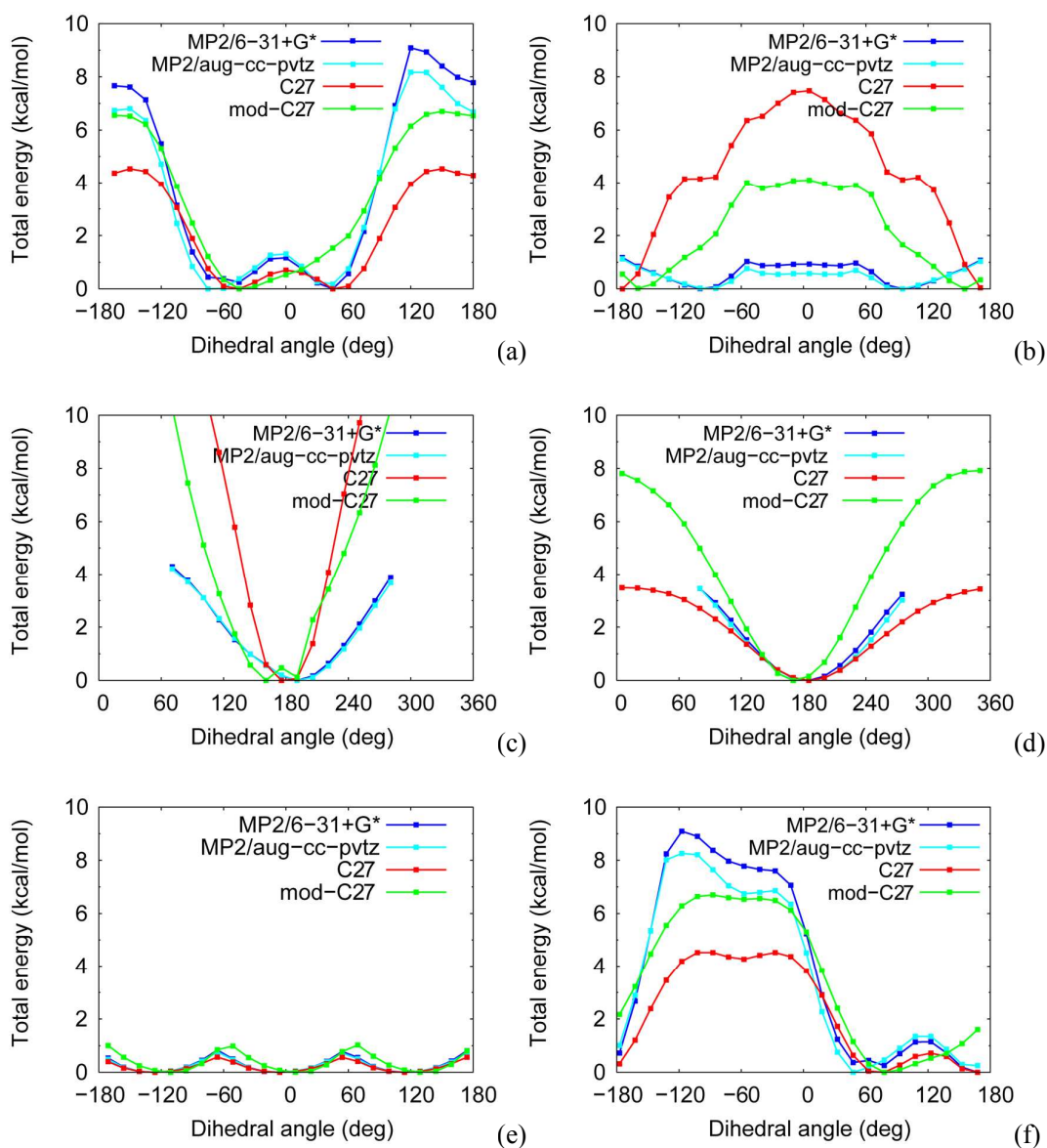
(c) REMD simulations of ATP in solution

	ATP in solution
Number of atoms	3404
Number of nucleotides	1ATP
Number of water molecules	1117
Number of counter ions	7K ⁺ , 3Cl ⁻
Box size (Å ³)	34 × 34 × 39

Table S2. Atom names, types and partial charges of methyl triphosphate (MTP).

Methyl triphosphate		
Atom name	Atom type	Partial charge
O1G	ON3	-0.90
O2G	ON3	-0.90
O3G	ON3	-0.90
PG	P2	1.10
O1B	ON3	-0.82
O2B	ON3	-0.82
O3B	ON2	-0.86
PB	P2	1.50
O1A	ON3	-0.82
O2A	ON3	-0.82
O3A	ON2	-0.74
PA	P	1.50
O5'	ON2	-0.62
C5'	CN9	-0.17
H15	HN9	0.09
H16	HN9	0.09
H17	HN9	0.09

Figure S1. Potential energy profiles along the selected dihedral angles of MTP calculated using both empirical force fields and *ab initio* methods: Modified CHARMM27 force-field (green), CHARMM27 force-field (red), MP2/6-31+G* (blue), and MP2/aug-cc-pVTZ//MP2/6-31+G* (cyan). Seven dihedral angles were considered: (a) C5'-O5'-PA-O3A, (b) O5'-PA-O3A-PB, (c) PA-O3A-PB-O3B, (d) O3A-PB-O3B-PG, (e) PB-O3B-PG-O1G, (f) C5'-O5'-PA-O1A, (g) PA-O3A-PB-O1B. The entire conformational space of the molecule was relaxed except for the dihedral angle of interest..



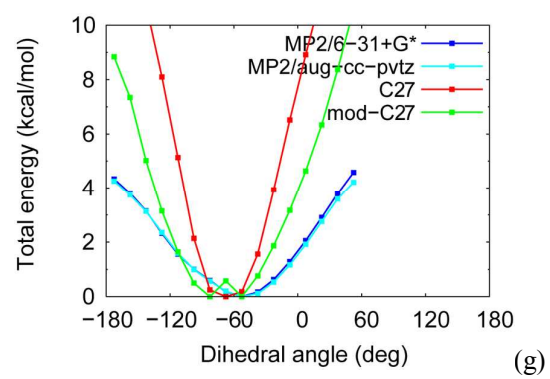


Figure S2. Time course of the selected structural parameters in 20 ns-MD simulations using mod-C27(ATP). Ion parameters of Merz, Jr.³ were used for Mg^{2+} and Ca^{2+} . (a) salt bridge (SB) distances: SB1 between α -phosphate and Arg489 (red line for C27(ATP) and green one for mod-C27(ATP)) and SB2 between β -phosphate and Arg560 (magenta for C27(ATP) and blue for mod-C27(ATP)). (b) RMSD of tri-phosphate moiety, (c) PA-O3A-PB bond angle, (d) O5'-PA-O3A-PB dihedral angle. The black lines in (c) and (d) show the corresponding distances observed in X-ray structure.

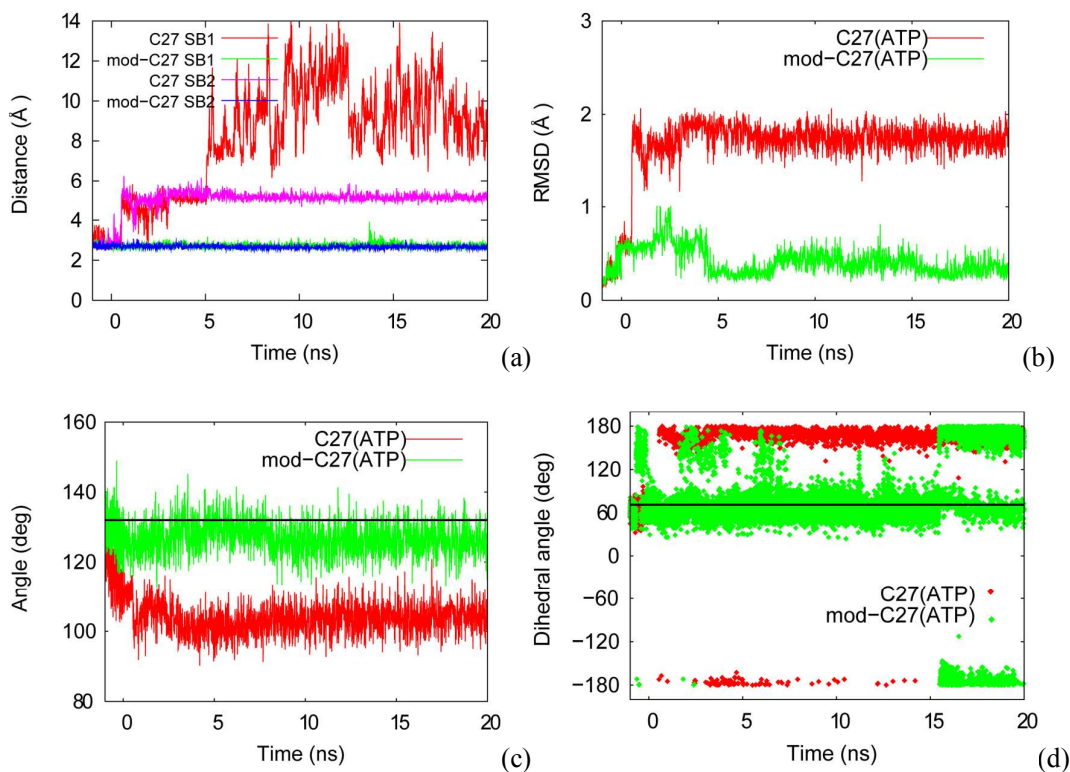


Figure S3. A snapshot of ATP-binding site after 20ns-MD simulation using mod-C27(ATP). Ion parameters of Merz, Jr.³ were used for Mg^{2+} and Ca^{2+} . The X-ray crystal structure of ATP bounded to Ca^{2+} -ATPase (gray) is shown for comparison.

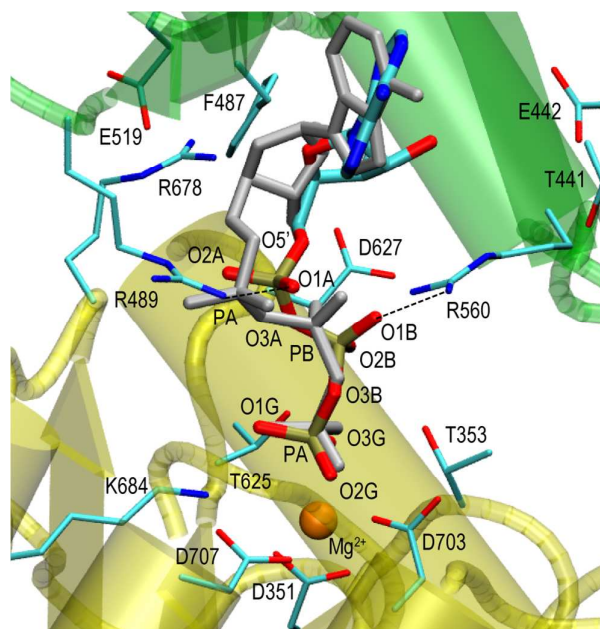


Figure S4. Root mean square deviations (RMSDs) of polyphosphate moiety of ATP for 5 ns MD simulations of ATP-bound proteins:

(a) Histidine permease (PDB: 1b0u), (b) RNA editing ligase MP52 (PDB entry: 1xdn), (c) Phosphoribosylamidoimidazole-succinocarboxamide synthase (PDB entry: 1obd), and (d) α -skeletal muscle Actin (PDB entry: 2fxu). RMSDs for the simulations with C27(ATP) and mod-C27(ATP) are shown in red and green, respectively.

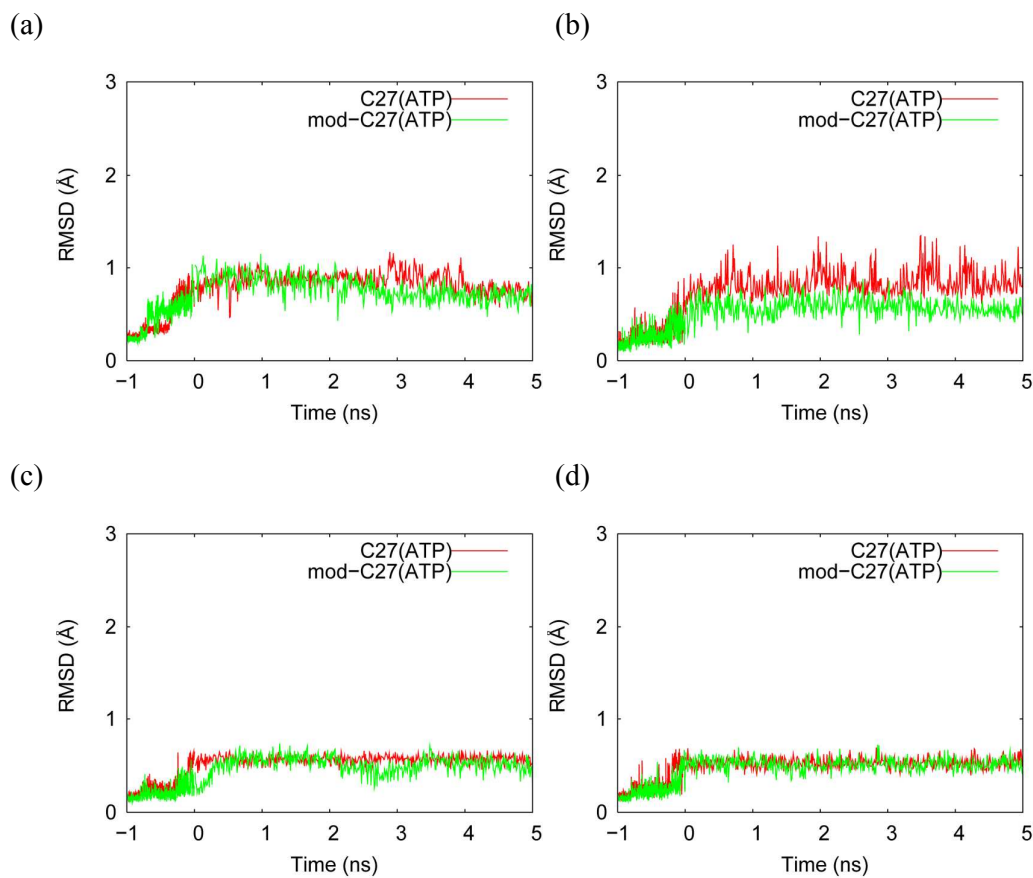
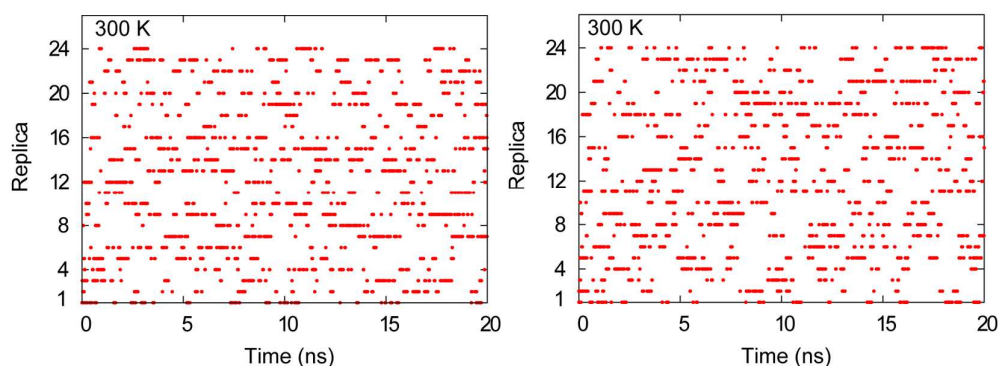
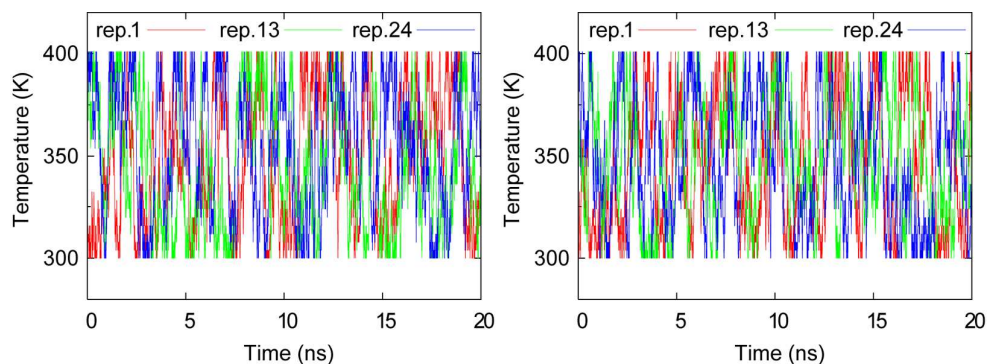


Figure S5. Performance of REMD simulations using C27(ATP) (left) and mod-C27(ATP) (right). (a) Time series of replica exchange at 300 K. (b) Time series of temperature exchange of three arbitrary chosen replicas (replica 1, 13, and 24). (c) Time series of total potential energy of three arbitrary chosen replicas (replica 1, 13, and 24). (d) The canonical probability distributions of the total potential energy of the system at 24 temperatures. 300 K, 350 K and 400 K are colored red, green and blue, respectively.

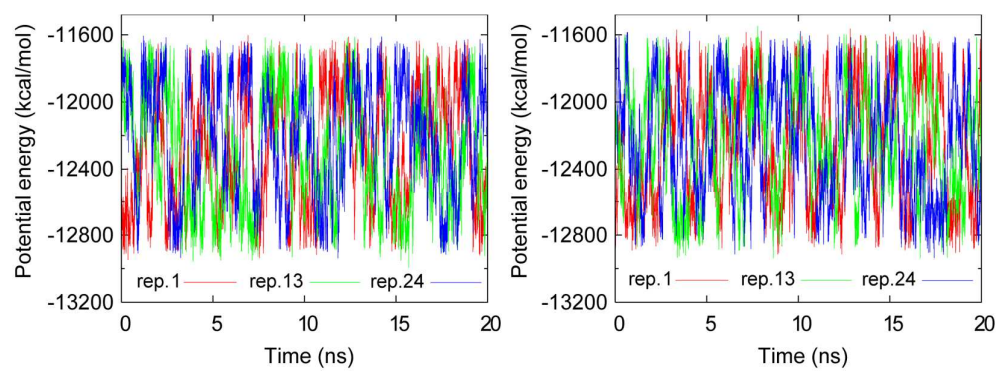
(a)



(b)



(c)



(d)

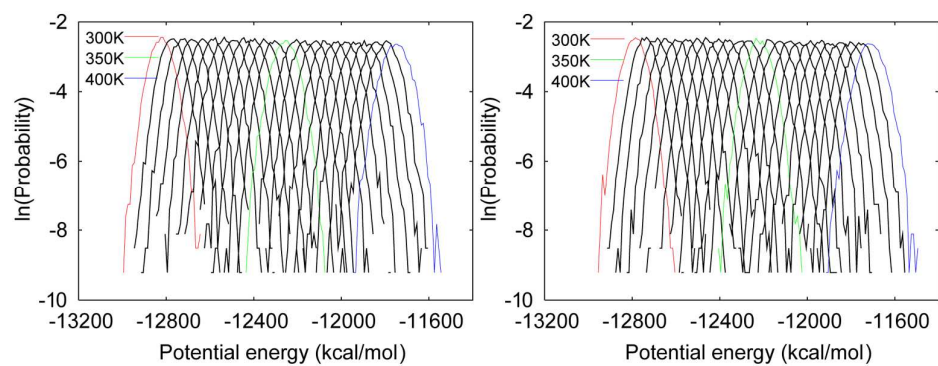


Figure S6. Convergence of REMD simulations using C27(ATP) (top) and mod-C27(ATP) (bottom). Cumulative averages of PMF landscapes along the two dihedral angles (O5'-PA-O3A-PB (**dih1**) and PA-O3A-PB-O3B (**dih2**)) are shown for every 5 ns.

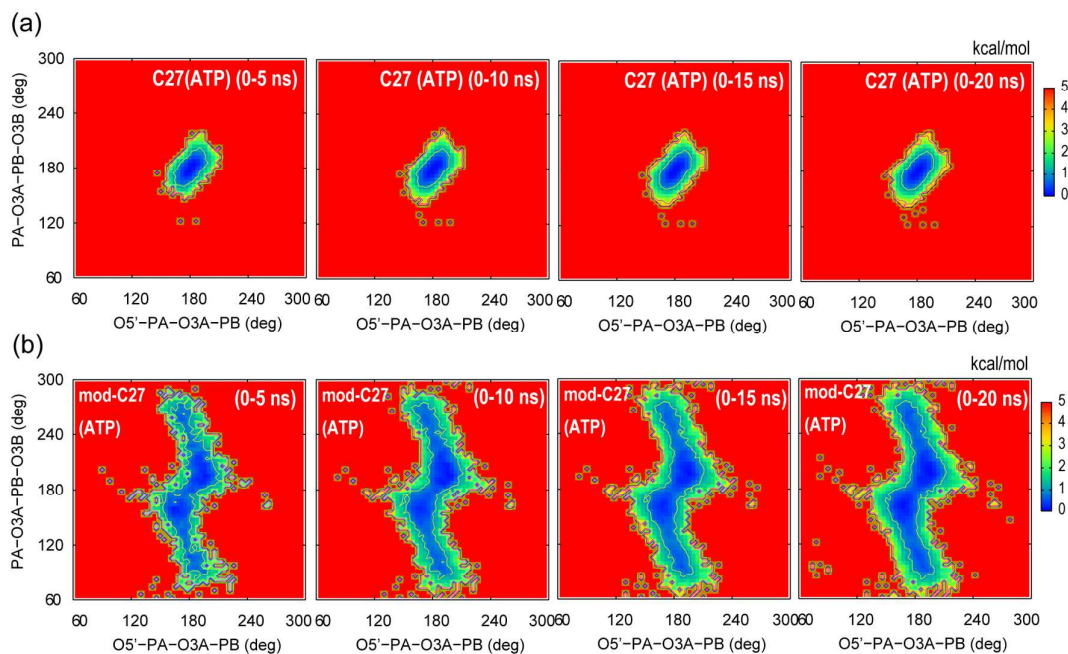
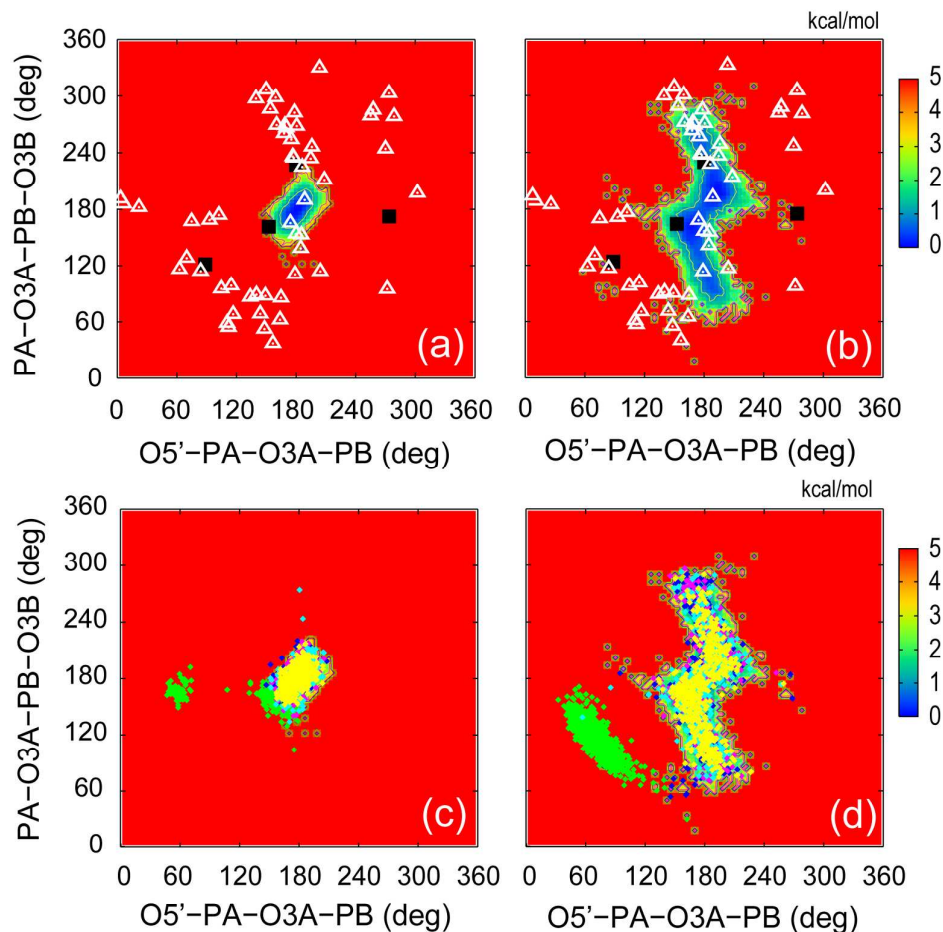


Figure S7. Comparison of calculated PMF with X-ray crystal structures. PMF landscapes along the O5'-PA-O3A-PB (**dih1**) and PA-O3A-PB-O3B (**dih2**) dihedral angles from the trajectory at 300 K in the REMD simulations using C27(ATP) (a) and mod-C27(ATP) (b). The corresponding values of 59 ATP structures in proteins, which were taken from Protein Data Bank (PDB), are marked on the PMF surfaces. Black squares are plotted for the crystal structures with resolutions better than 1.5 Å (4 structures), while white triangles are plotted for the structure with resolutions between 1.5 Å and 2.0 Å (55 structures). The **dih1-dih2** distribution maps for the simulations of Ca²⁺-ATPase (green) as well as additional four ATP-binding proteins (blue for Histidine permease, magenta for RNA editing ligase MP52, cyan for Phosphoribosylamidoimidazole-succinocarboxamide synthase, and yellow for α -skeletal muscle Actin) using C27(ATP) and mod-C27(ATP) are shown in (c) and (d), respectively.



REFERENCES

1. Humphrey, W.; Dalke, A.; Schulten, K., VMD: Visual molecular dynamics. *J. Mol. Graph.* **1996**, *14*, 33-38.
2. Gumbart, J.; Trabuco, L. G.; Schreiner, E.; Villa, E.; Schulten, K., Regulation of the protein-conducting channel by a bound ribosome. *Structure* **2009**, *17*, 1453-1464.
3. Li, P.; Roberts, B. P.; Chakravorty, D. K.; Merz, K. M., Jr., Rational Design of Particle Mesh Ewald Compatible Lennard-Jones Parameters for +2 Metal Cations in Explicit Solvent. *J. Chem. Theory Comput.* **2013**, *9*, 2733-2748.